Letter

Interaction shift of the Bose-Einstein condensation temperature in a dipolar gas

Milan Krstajić, Jiří Kučera, Lucas R. Hofer, Gavin Lamb, Péter Juhász, and Robert P. Smith*
Clarendon Laboratory, University of Oxford, Parks Road, Oxford OX1 3PU, United Kingdom

(Received 31 January 2025; accepted 5 May 2025; published 19 May 2025)

We report measurements of the Bose-Einstein condensate critical temperature shift due to dipolar interactions, employing samples of ultracold erbium atoms which feature significant (magnetic) dipole-dipole interactions in addition to tunable contact interactions. Using a highly prolate harmonic trapping potential, we observe a clear dependence of the critical temperature on the orientation of the dipoles relative to the trap axis. Our results are in good agreement with mean-field theory for a range of contact interaction strengths. This work creates an opportunity for further investigations into beyond-mean-field effects and the finite-temperature phase diagram in the more strongly dipolar regime where supersolid and droplet states emerge.

DOI: 10.1103/PhysRevA.111.L051303

The phase transition to a Bose-Einstein condensate (BEC) is unique in that it is not driven by interactions but can occur solely due to quantum statistics. However, in the myriad of systems and phenomena where Bose condensation plays a critical role—from superconductivity to liquid helium to exciton and magnon condensation—interparticle interactions are always present and often strong. The interplay of interactions and Bose condensation is thus an important one, and an obvious question concerns the effect of interactions on the critical point. Surprisingly, even for weak short-range interactions, this is a theoretically difficult question to answer due to nonperturbative correlations that develop near the critical point. The conclusion (after a 50-year-long theoretical debate) was that for a homogeneous system, repulsive contact interactions enhance condensation, i.e., lead to a positive shift of the transition temperature [1–5].

Ultracold gases provide an ideal setting in which to experimentally address such questions. However, the finite (and often inhomogeneous) traps used to confine these gases further complicate the picture. In the case of a harmonically trapped gas with repulsive contact interactions, there is a geometric mean-field effect which reduces the critical temperature T_c [6]. Measurements, utilizing tunable interactions in a potassium gas, showed agreement with this mean-field prediction for weak interactions as well as evidence of an upturn at stronger interactions due to beyond-mean-field effects [7].

The physics becomes even richer when going beyond just contact interactions. In particular, experiments on ultracold atoms that additionally experience dipole-dipole interactions (DDI) have uncovered new single-droplet [8], droplet-array [9,10], and supersolid phases [11–14], alongside the usual BEC. However, these experiments mostly focused on the zero-temperature regime, and the effect of dipolar interactions on the transition temperature (to a BEC or more exotic phases) has not been measured.

In this Letter, we report measurements of the BEC critical temperature shift due to dipolar interactions. Using an ultracold dipolar Bose gas of ^{166}Er atoms in a cigar-shaped harmonic trap, we reveal how T_c depends on both the orientation of the dipoles (relative to the trap axis) and the relative strength of dipolar and contact interactions. Our results show a clear dipolar effect that is broadly in line with mean-field theoretical predictions [15,16] and also begin to explore the region where such predictions may no longer be valid.

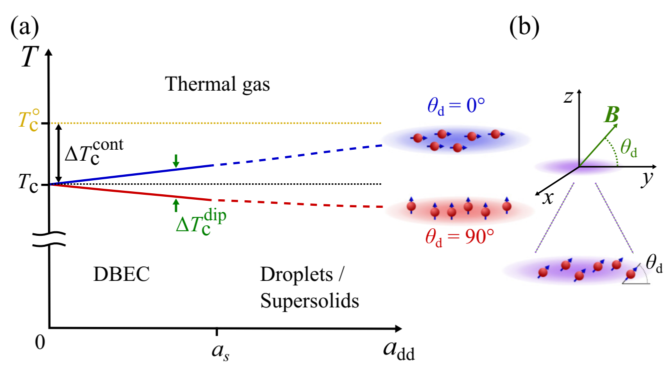

FIG. 1. Dipolar T_c shift. (a) Cartoon phase diagram for a dipolar Bose gas showing the transition temperature T_c between the thermal gas and the condensed phase. Depending on the value of the dipolar length a_{dd}, the degenerate gas either will be in the dipolar BEC state (DBEC) or for $a_{dd} \gtrsim a_s$ may collapse and form a dipolar droplet or supersolid phase. Repulsive contact interactions alone (black dotted line) cause T_c to reduce by ΔT_c^{cont} compared to the ideal gas case T_c°(yellow dotted line). The DDI are predicted to further modify T_c with the sign and magnitude depending on the dipole orientation. (b) The dipole orientation is set by the direction of the magnetic field **B**, which can be freely varied in the $y - z$ plane, changing the tilt angle θ_d with respect to the trap's long (y) axis.

*Contact author: robert.smith@physics.ox.ac.uk

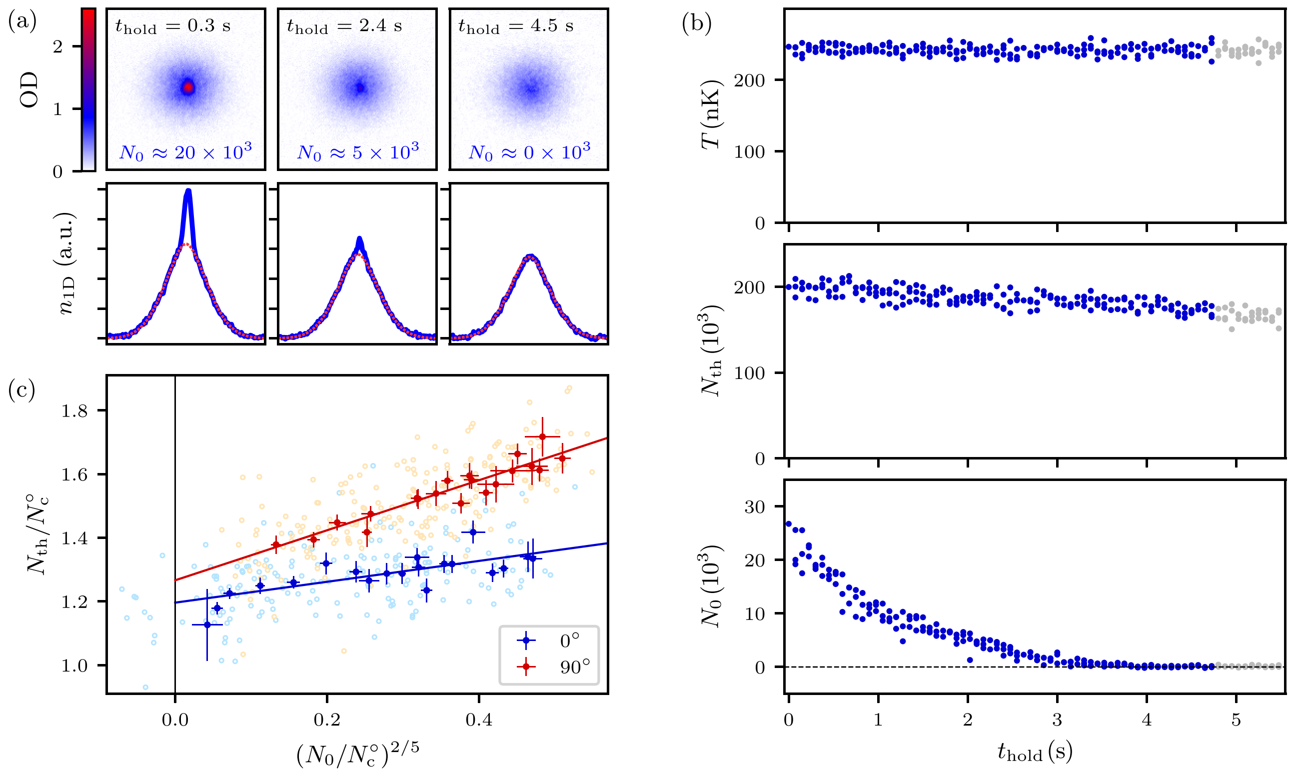

FIG. 2. Example of a critical point measurement. Here a harmonic trap with frequencies $(\omega_x, \omega_y, \omega_z) = 2\pi \times (294, 14.0, 233)$ Hz was used and $a_s = 72a_0$. (a) Absorption images and corresponding 1D sums of $\theta_d = 0^\circ$ clouds at three different hold times. The red lines are fits of the Bose distribution to the thermal component. (b) Dependence of temperature, and thermal and condensate atom number (extracted from the absorption images) versus hold time for $\theta_d = 0^\circ$. The data where we can confidently determine that no condensate is present (gray points) are filtered out before further analysis [17]. (c) Dependence of N_{th} on N_0 for $\theta_d \in \{0^\circ, 90^\circ\}$. To accommodate negative N_0 values, which occur due to fitting noise, we use $N_0^{2/5} = \text{sgn}(N_0)|N_0|^{2/5}$. The open circles show individual data points and the closed circles represent binned data. The intercepts of the linear fits give the critical atom number N_c and the gradients the magnitude S of the nonsaturation effect. Note that small negative N_0 values [in both (b) and (c)] arise due to noise on our optical density (OD) images [17].

Figure 1 summarizes the mean-field effect of both contact and dipolar interactions on the BEC critical point in an anisotropic harmonic trap; for simplicity, we consider a cylindrically symmetric trap (with frequencies $\omega_\parallel$ and $\omega_\perp$). In this trap, an ideal gas with a fixed particle number N has a critical temperature (yellow dotted line) given by $k_B T_c^\circ = \hbar\bar{\omega}[N\bar{\omega}/\zeta(3)]^{1/3}$, where $\bar{\omega} = (\omega_\parallel \omega_\perp^2)^{1/3}$ is the geometric mean of the trapping frequencies and ζ is the Riemann zeta function. The shift in T_c, in the mean-field approximation, is given by [15]

$$\frac{\Delta T_c}{T_c^\circ} = -3.426\frac{a_s}{\lambda} + 3.426\frac{a_{dd}}{\lambda} f\left(\frac{\omega_\parallel}{\omega_\perp}\right)\frac{3\cos^2\theta_d - 1}{4}. \quad (1)$$

The first term on the right-hand side arises due to contact interactions; this shift ΔT_c^{cont} is negative and proportional to the ratio of the s-wave scattering length a_s and the thermal wavelength $\lambda = \sqrt{2\pi\hbar^2/mk_B T_c^\circ}$, where m is the particle mass. The second term describes the effect of DDI with strength characterized by the dipolar length $a_{dd} = \mu_0\mu_d^2 m/12\pi\hbar^2$; here μ_d is the magnetic moment of each atom. The anisotropic nature of the dipolar interactions means that the shift additionally depends on both the angle of the dipole orientation relative to the trap symmetry axis (θ_d) and the aspect ratio of the trap. The function $f(\omega_\parallel/\omega_\perp)$, defined in [15] (see also [17]), is approximately equal to 1 for the highly prolate cigar-shaped traps ($\omega_\parallel \ll \omega_\perp$) used in this work.

If one instead considers a system at fixed temperature, which is often more experimentally achievable than the fixed N case, the ideal critical atom number is given by $N_c^\circ = \zeta(3)(k_B T_c^\circ/\hbar\bar{\omega})^3$ and any (small) shifts are related to Eq. (1) via

$$\frac{\Delta N_c}{N_c^\circ} = -3\frac{\Delta T_c}{T_c^\circ}. \quad (2)$$

The fixed-temperature scenario also highlights a further important effect of interactions on Bose condensation, namely, nonsaturation. If N is increased beyond N_c, a condensate forms but the thermal component of the gas fails to saturate at $N_{\text{th}} = N_c$ and instead continues growing with increasing condensate number N_0. This effect, which has been demonstrated for Bose gases with only contact interactions [23], makes the measurement of the critical point more challenging, as the critical atom number N_c can no longer be identified with N_{th} in a gas with (any) finite condensed fraction. Consequently, the $N_c = N_{\text{th}}$ condition holds only at the transition point itself and one must therefore carefully extrapolate to $N_0 \to 0$.

Our experiments use a gas of magnetically dipolar ^{166}Er atoms, in the lowest Zeeman sublevel, for which $a_{dd} = 65.4a_0$ (with a_0 the Bohr radius) and a_s can be tuned using a low-field (approximately equal to 0 G) Feshbach resonance [24]; the relatively modest a_{dd} is only expected to lead to dipolar effects on T_c at the few percent level, providing a significant experimental challenge. Our approach to this is to perform differential measurements whereby one seeks to directly measure the change in T_c due to changes in θ_d and a_s while keeping everything else the same. This results in the cancellation of most first-order common-mode systematic errors, e.g., on the atom number, trap frequencies,[1] and temperature.

We begin by preparing [26] a partially condensed cloud in our cigar-shaped optical dipole trap and with a magnetic field of $B = 1.4$ G ($a_s = 72a_0$) applied perpendicular to the trap axis. We then rotate the magnetic field to set the desired θ_d and subsequently ramp the magnetic field to its final value to set a_s. To vary N, we introduce a variable hold time t_{hold} during which the trap depth is chosen to ensure the temperature remains constant.[2] Finally, we turn off the trap and use absorption imaging on the broad 401-nm transition to record atomic density profiles after (18–24)-ms time-of-flight (TOF) expansion. For a given data run, we perform three interleaved sets of measurements: two at our chosen a_s at both $\theta_d = 0^\circ$ and 90° and one calibration series with $a_s = 72a_0$ and $\theta_d = 90^\circ$. The calibration series effectively allows us to perform a differential measurement with respect to the same (fixed) point; see the Supplemental Material [17] for more details.

Figure 2(a) shows example images, as well as corresponding integrated one-dimensional (1D) density profiles, for three different hold times for our data series with $a_s = 72a_0$ and $\theta_d = 0^\circ$. From the images we obtain the data triplet of (T, N_{th}, N_0) [17]. Note that the effect of interactions on the atom cloud during TOF (and thus the fitted temperature) depends on the dipole orientation (and a_s) [27]. So, as they are not common mode, we correct for these effects (see [17]). In Fig. 2(b) we show how the three extracted quantities vary with t_{hold}. We see that the temperature remains essentially constant while the atom number slowly decays and N_0 decreases, eventually reaching zero.

To determine the critical atom number, taking nonsaturation effects into account, we plot N_{th} versus $N_0^{2/5}$ [shown in Fig. 2(c) for $a_s = 72a_0$ and $\theta_d = \{0^\circ, 90^\circ\}$]. Plotting this way allows a linear extrapolation to $N_0 \to 0$ for a purely contact interacting gas [23] and we have numerically shown that for $\varepsilon_{dd} = a_{dd}/a_s < 1$ this remains true in the presence of dipolar interactions (see [17]). To take any small (less than 10%) variations of T into account, we scale both N_{th} and N_0 by

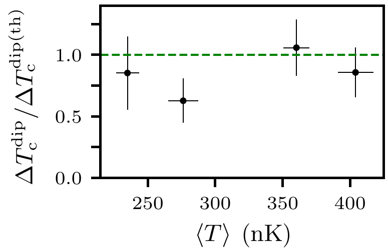

$\langle T \rangle$ [nK]	ω_x	ω_y [2π Hz]	ω_z
235(9)	294	14.0	233
276(11)	257	32.0	218
360(10)	312	26.9	269
404(13)	311	20.5	270

FIG. 3. Dipolar T_c shift at $\varepsilon_{dd} = 0.91$ versus cloud temperature. The plot shows the ratio of ΔT_c^{dip} to the mean-field theoretical prediction; $\langle T \rangle$ is the mean temperature for each data series. The table shows the trapping frequencies used in each case.

$N_c^\circ(T)$. Even without fitting the data, we see a clear effect of dipole orientation on the thermodynamics of the BEC critical point.

Before performing a linear fit to the data in Fig. 2(c), the effect of random measurement and fitting noise needs to be considered carefully due to several subtle effects. First, the presence of random noise in estimating N_0 and T skews the linear fit due to the strongly nonlinear power-law scaling of $(N_0/N_c^\circ)^{2/5}$. To mitigate this, we bin raw data points, grouping them by t_{hold} (see [17] for further details), to produce the solid points in Fig. 2(c). Second, as significant errors are present in both the x- and y-axis variables, we utilize orthogonal distance regression [28] when performing the linear fits. These fits yield a slope S and an intercept N_c/N_c°; the transition temperature shift is then [see Eq. (2)] given by $\Delta T_c/T_c^\circ = -\frac{1}{3}(N_c/N_c^\circ - 1)$.

To isolate the effect of the DDI on the transition temperature, evident in the different intercepts in Fig. 2(c), we also calculate

$$\Delta T_c^{dip} = \Delta T_c|_{\theta_d=0^\circ} - \Delta T_c|_{\theta_d=90^\circ}, \tag{3}$$

which for the data in Fig. 2(c) gives $\Delta T_c^{dip}/T_c^\circ = 2.3(0.9)\%$, in good agreement with the mean-field prediction of 2.7%. To confirm the robustness of this result at $a_s = 72a_0$ ($\varepsilon_{dd} = 0.91$), we performed similar measurements at three additional configurations with different cloud temperatures and trap shapes. These data are shown in Fig. 3, which confirms the overall good agreement with the mean-field prediction.

Finally, in Fig. 4 we explore the effect of varying a_s on T_c. Figure 4(a) shows $\Delta T_c/T_c^\circ$ versus a_s/λ for $\theta_d = 0^\circ$ and 90°.[3] The solid lines are the dipolar shift predicted by Eq. (3)

[1]Note that, due to the tensor polarizability of erbium, a change in the dipole orientation can lead to a change in the trap frequencies. To compensate, we carefully measured the effect, allowing us to appropriately adjust the optical dipole trap laser power during dipole rotations. Our measurements are consistent with the theoretically predicted tensor part of the polarizability [25].

[2]Note that the hold time is either immediately before or after the B-field ramp. Also note that the constant temperature comes about due to a balance between heating (e.g., due to inelastic collisions or one-body trap heating) and residual evaporation.

[3]Note that to extract ΔT_c (the shift from the noninteracting limit), we assume that ΔT_c of our calibration data is given by the first-order mean-field result (cf. Fig. 3 and [17]); we emphasize that any breakdown of this assumption would *only* result in a global (vertical) shift of all the data in Fig. 4(a).

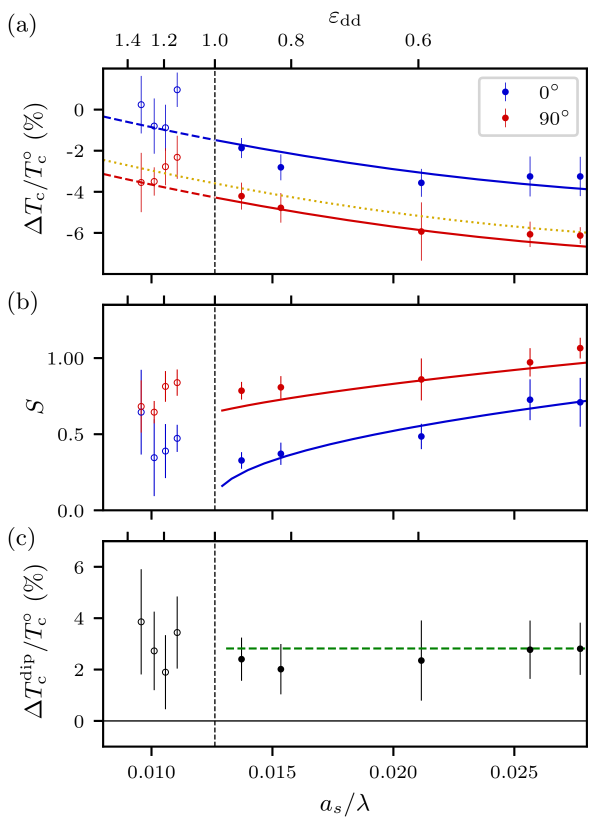

FIG. 4. Critical temperature shift in a dipolar gas. (a) Plot of ΔT_c, at different values of the scattering length a_s and for $\theta_d = 0^\circ$ and $\theta_d = 90^\circ$. Measurements were performed in the same trap as in Fig. 2. [We note that while $\Delta T_c/T_c^0$ is expected to depend only on a_s/λ and a_{dd}/λ, as all points have essentially the same temperature (235 nK) and fixed a_{dd}, we add a (secondary) ε_{dd} axis for reference.] The lines represent the theoretical expectation (see the text for details): blue solid for $\theta_d = 0^\circ$, red solid for $\theta_d = 90^\circ$, and yellow dotted for a nondipolar gas (cf. Fig. 1). (b) Measured slopes of the nonsaturation effect compared with mean-field numerical predictions based on the Thomas-Fermi approximation (which only gives a stable solution for $\varepsilon_{dd} < 1$). (c) Dipolar contribution to ΔT_c, which is simply the difference between the red and blue data points in (a). The green dashed line represents the mean-field theoretical prediction for ΔT_c^{dip}. The open symbols denote points where $\varepsilon_{dd} > 1$; here the extrapolation procedure for extracting N_c (based on a fit of N_{th} vs $N_0^{2/5}$) may no longer be theoretically justified even though empirically it still describes the data well.

together with the previously measured contact interaction shift [7] [which includes a term quadratic in a_s/λ as well as the linear term in Eq. (3)]; our data show close alignment with this prediction.

Figure 4(b) displays the fitted slopes for the same data, which also show good agreement with our calculated nonsaturation slopes (solid lines). The calculations employ the mean-field model from Ref. [23] with dipolar interactions included (see [17] for details); note that they cannot be performed for $\varepsilon_{dd} > 1$, as in this regime the gas is unstable within the Thomas-Fermi approximation.

Finally, in Fig. 4(c) we plot ΔT_c^{dip}, highlighting the clear shift of the BEC transition temperature due to dipolar interactions across a range of a_s and the very good agreement with mean-field predictions (green dashed line) for $\varepsilon_{dd} < 1$ [15,16].

We now briefly consider the region $\varepsilon_{dd} > 1$, where the mean-field theory is expected to break down and where the ground state may not be a "standard" BEC but rather a droplet or supersolid state that is stabilized by beyond-mean-field effects. Here we limit ourselves to modest values of ε_{dd} to ensure that our measurements remain close to equilibrium (the three-body loss rate grows sharply as a_s is reduced [26]). In this so-called strongly dipolar regime, the linear N_{th} versus $N_0^{2/5}$ trend is no longer expected to hold. However, we empirically find that it still describes the data well. We find that the T_c values obtained using this approach broadly follow the extrapolated mean-field predictions. Future investigations of the strongly dipolar regime will require a careful choice of trap parameters to ensure equilibrium conditions and an improved understanding of the consequences of the new ground states on the nonsaturation effect.

In conclusion, we performed a high-precision study of the BEC transition temperature in an ultracold dipolar gas with a range of contact interaction strengths. Our results show a clear effect of dipolar interactions on the transition temperature. This is most clearly seen by directly comparing the T_c for clouds with the dipoles orientated parallel and perpendicular to the axis of the cigar-shaped trap confining the atoms. The magnitude of the effect is in good agreement with mean-field predictions.

In the future, it would be interesting to explore the more strongly dipolar regime where beyond-mean-field effects are expected to become important. For example, recent studies have suggested that quantum fluctuations can significantly shift the finite-temperature phase boundary between the superfluid and supersolid states [29–33]. We also note that the use of more homogeneous traps [34] should make these beyond mean-field effects more resolvable.

We thank Christoph Eigen and Zoran Hadzibabic for comments on the manuscript and Joanne Roper for her contribution to evaluating the temperature corrections. This work was supported by the UK EPSRC (Grants No. EP/P009565/1 and No. EP/T019913/1). R.P.S. and P.J. acknowledge support from the Royal Society; P.J. acknowledges support from the Hungarian National Young Talents Scholarship; M.K. acknowledges support from Trinity College, Cambridge; J.K. acknowledges support from the Oxford Physics Endowment for Graduates; L.R.H. acknowledges support from Christ Church College, Oxford; and G.L. acknowledges support from Wolfson College, Oxford.

Data availability. The data that support the findings of this article are openly available [35].

[1] J. O. Andersen, Theory of the weakly interacting Bose gas, Rev. Mod. Phys. **76**, 599 (2004).

[2] P. Arnold and G. Moore, BEC transition temperature of a dilute homogeneous imperfect Bose gas, Phys. Rev. Lett. **87**, 120401 (2001).

[3] G. Baym, J.-P. Blaizot, M. Holzmann, F. Laloë, and D. Vautherin, Bose–Einstein transition in a dilute interacting gas, Eur. Phys. J. B **24**, 107 (2001).

[4] M. Holzmann, J.-N. Fuchs, G. A. Baym, J.-P. Blaizot, and F. Laloë, Bose–Einstein transition temperature in a dilute repulsive gas, C. R. Phys. **5**, 21 (2004).

[5] V. A. Kashurnikov, N. V. Prokof'ev, and B. V. Svistunov, Critical temperature shift in weakly interacting Bose gas, Phys. Rev. Lett. **87**, 120402 (2001).

[6] S. Giorgini, L. P. Pitaevskii, and S. Stringari, Condensate fraction and critical temperature of a trapped interacting Bose gas, Phys. Rev. A **54**, R4633(R) (1996).

[7] R. P. Smith, R. L. D. Campbell, N. Tammuz, and Z. Hadzibabic, Effects of interactions on the critical temperature of a trapped Bose gas, Phys. Rev. Lett. **106**, 250403 (2011).

[8] L. Chomaz, S. Baier, D. Petter, M. J. Mark, F. Wächtler, L. Santos, and F. Ferlaino, Quantum-fluctuation-driven crossover from a dilute Bose-Einstein condensate to a macrodroplet in a dipolar quantum fluid, Phys. Rev. X **6**, 041039 (2016).

[9] H. Kadau, M. Schmitt, M. Wenzel, C. Wink, T. Maier, I. Ferrier-Barbut, and T. Pfau, Observing the Rosensweig instability of a quantum ferrofluid, Nature (London) **530**, 194 (2016).

[10] I. Ferrier-Barbut, H. Kadau, M. Schmitt, M. Wenzel, and T. Pfau, Observation of quantum droplets in a strongly dipolar Bose gas, Phys. Rev. Lett. **116**, 215301 (2016).

[11] F. Böttcher, J.-N. Schmidt, M. Wenzel, J. Hertkorn, M. Guo, T. Langen, and T. Pfau, Transient supersolid properties in an array of dipolar quantum droplets, Phys. Rev. X **9**, 011051 (2019).

[12] L. Tanzi, E. Lucioni, F. Famà, J. Catani, A. Fioretti, C. Gabbanini, R. N. Bisset, L. Santos, and G. Modugno, Observation of a dipolar quantum gas with metastable supersolid properties, Phys. Rev. Lett. **122**, 130405 (2019).

[13] L. Chomaz, D. Petter, P. Ilzhöfer, G. Natale, A. Trautmann, C. Politi, G. Durastante, R. M. W. van Bijnen, A. Patscheider, M. Sohmen, M. J. Mark, and F. Ferlaino, Long-lived and transient supersolid behaviors in dipolar quantum gases, Phys. Rev. X **9**, 021012 (2019).

[14] M. Sohmen, C. Politi, L. Klaus, L. Chomaz, M. J. Mark, M. A. Norcia, and F. Ferlaino, Birth, life, and death of a dipolar supersolid, Phys. Rev. Lett. **126**, 233401 (2021).

[15] K. Glaum, A. Pelster, H. Kleinert, and T. Pfau, Critical temperature of weakly interacting dipolar condensates, Phys. Rev. Lett. **98**, 080407 (2007).

[16] K. Glaum and A. Pelster, Bose-Einstein condensation temperature of dipolar gas in anisotropic harmonic trap, Phys. Rev. A **76**, 023604 (2007).

[17] See Supplemental Material at http://link.aps.org/supplemental/10.1103/PhysRevA.111.L051303 for more details on data acquisition, data processing, calibration procedure, and systematic error mitigation and for an outline of the mathematical apparatus needed to calculate the nonsaturation effect in dipolar BECs, which includes Refs. [18–22].

[18] L. R. Hofer, M. Krstajić, and R. P. Smith, JAXFit: Trust region method for nonlinear least-squares curve fitting on the GPU, arXiv:2208.12187.

[19] L. Verlet, Computer "experiments" on classical fluids. I. Thermodynamical properties of Lennard-Jones molecules, Phys. Rev. **159**, 98 (1967).

[20] S. Giovanazzi, P. Pedri, L. Santos, A. Griesmaier, M. Fattori, T. Koch, J. Stuhler, and T. Pfau, Expansion dynamics of a dipolar Bose-Einstein condensate, Phys. Rev. A **74**, 013621 (2006).

[21] C. J. Pethick and H. Smith, *Bose-Einstein Condensation in Dilute Gases* (Cambridge University Press, Cambridge, 2002).

[22] C. Eberlein, S. Giovanazzi, and D. H. J. O'Dell, Exact solution of the Thomas-Fermi equation for a trapped Bose-Einstein condensate with dipole-dipole interactions, Phys. Rev. A **71**, 033618 (2005).

[23] N. Tammuz, R. P. Smith, R. L. D. Campbell, S. Beattie, S. Moulder, J. Dalibard, and Z. Hadzibabic, Can a Bose gas be saturated? Phys. Rev. Lett. **106**, 230401 (2011).

[24] A. Patscheider, L. Chomaz, G. Natale, D. Petter, M. J. Mark, S. Baier, B. Yang, R. R. W. Wang, J. L. Bohn, and F. Ferlaino, Determination of the scattering length of erbium atoms, Phys. Rev. A **105**, 063307 (2022).

[25] J. H. Becher, S. Baier, K. Aikawa, M. Lepers, J.-F. Wyart, O. Dulieu, and F. Ferlaino, Anisotropic polarizability of erbium atoms, Phys. Rev. A **97**, 012509 (2018).

[26] M. Krstajić, P. Juhász, J. Kučera, L. R. Hofer, G. Lamb, A. L. Marchant, and R. P. Smith, Characterization of three-body loss in ^{166}Er and optimized production of large Bose-Einstein condensates, Phys. Rev. A **108**, 063301 (2023).

[27] Y. Tang, A. G. Sykes, N. Q. Burdick, J. M. DiSciacca, D. S. Petrov, and B. L. Lev, Anisotropic expansion of a thermal dipolar Bose gas, Phys. Rev. Lett. **117**, 155301 (2016).

[28] P. T. Boggs and J. E. Rogers, Statistical analysis of measurement error models and applications, in *Proceedings of the AMS-IMS-SIAM Joint Summer Research Conference*, edited by P. J. Brown and W. A. Fuller (AMS, Providence, 1990).

[29] E. Aybar and M. O. Oktel, Temperature-dependent density profiles of dipolar droplets, Phys. Rev. A **99**, 013620 (2019).

[30] J. Sánchez-Baena, C. Politi, F. Maucher, F. Ferlaino, and T. Pohl, Heating a dipolar quantum fluid into a solid, Nat. Commun. **14**, 1868 (2023).

[31] J. Sánchez-Baena, T. Pohl, and F. Maucher, Superfluid-supersolid phase transition of elongated dipolar Bose-Einstein condensates at finite temperatures, Phys. Rev. Res. **6**, 023183 (2024).

[32] L.-J. He, F. Maucher, and Y.-C. Zhang, Infrared cutoff for dipolar droplets, Phys. Rev. A **110**, 053316 (2024).

[33] L.-J. He, J. Sánchez-Baena, F. Maucher, and Y.-C. Zhang, Accessing elusive two-dimensional phases of dipolar Bose-Einstein condensates by finite temperature, Phys. Rev. Res. **7**, 023019 (2025).

[34] P. Juhász, M. Krstajić, D. Strachan, E. Gandar, and R. P. Smith, How to realize a homogeneous dipolar Bose gas in the roton regime, Phys. Rev. A **105**, L061301 (2022).

[35] R. Smith, Data Associated with the Publication 'Interaction Shift of the Bose-Einstein Condensation Temperature in a Dipolar Gas' (University of Oxford, 2025), https://dx.doi.org/10.5287/ora-m8gpvdr2y.